Pipe Data Through the Water: Stress Wave Communications Along Pipelines

Debing Wei
University of Houston
dwei3@uh.edu

Chaoxian Qi
University of Houston
cqi4@uh.edu

Jiefu Chen
University of Houston
jchen84@uh.edu

Aijun Song
University of Alabama
song@eng.ua.edu

Gangbing Song
University of Houston
gsong@uh.edu

Miao Pan
University of Houston
mpan2@uh.edu

ABSTRACT

Offshore pipelines are the most popular man-made infrastructures that can be found undersea. Empowered by stress wave communications, these massive pipeline networks can be potentially utilized to deliver information. In this paper, we build up a stress wave communication system along a ten feet steel pipe. The communication performances were tested undersea. Based on our testing data, the potentials of this new subsea communication technique are discussed.

KEYWORDS

Stress Wave; Pipeline; Communication; Subsea.

1 INTRODUCTION

Offshore pipeline is considered to be the most efficient and effective modes of transport for carbon products. Owing to the escalating demand for oil and gas, thousands of miles of offshore pipelines have been deployed all over the world. Taking the Gulf of Mexico as an example, over 44,000 miles of pipelines have been deployed during the last century [1]. The State of the Coast website boasts of the US National Oceanic and Atmospheric Administration (NOAA), "If placed end to end, the oil and gas pipelines in the Gulf of Mexico could wrap around the Earth's equator.". The lifespan of offshore pipeline is around 40 years. By far, a large portion of offshore pipelines are out of service. For example, there are more than 18,000 miles of "out of service" pipelines in the Gulf of Mexico [2]. Since these offshore pipelines are directly connected to the onshore facilities, we proposed to utilize these unused offshore pipelines as a propagation medium and apply stress wave waveguide technology for subsea data transmissions.

In comparison with acoustic wireless communications, this new type of stress wave communications (SWC) has many advantages. First, the propagation velocity of stress wave along a steel pipe is around 5500 m/s which is over 3 times faster than the speed of acoustic wave. Hence, smaller communication delay can be expected. Second, the acoustic wave suffers from geometric spreading loss since the sound energy is radiated equally in all directions. On the contrary, the propagation of stress wave is only along one dimension, so that no geometric spreading loss needs to be concerned. Thus, the power consumption for SWC can be much smaller than acoustic communications. Third, unlike the acoustic channel which is strongly affected by the surrounding environments, e.g. pressure and temperature, the stress wave channel is much more stable and robust. This is because once the transmitter and receiver were located on the pipe, the stress wave channel condition would be deterministic. Therefore, highly reliable data transmissions can be realized through SWC with small channel error rates.

Besides acoustic signals, electromagnetic signals are the most popular physical signals that can be used for wireless communications. But due to the high conductivity of sea water, the radio frequency signals with frequency higher than MHz almost cannot work subsea due to the high attenuation rate. Recently, the Magnetic Induction (MI) technique which rely on the quasi-static magnetic fields were investigated for underwater wireless communications [3–6]. Both the theoretical studies and field tests [7] suggest that the subsea communication range of MI wireless communications is within several meters. In comparison with subsea MI wireless communications, SWC can work within the similar spectrum range around hundreds of KHz. But the communication range for SWC would be much longer depending on the length of pipelines.

To our knowledge, this is the first attempt to investigate the SWC on offshore pipelines. But a couple of researchers has demonstrated SWC on some other solid mediums with different titles of this technology. Creig. C Johnson [8] had demonstrated seismic communications with a data rate of 2 pulse per second at a distance of 760 ft through hard rocks back in 1972. Lawry et al. [9] presents a system capable of high data-rate transmission through solid metal barriers using ultrasound. The proposed prototype has realized 12.4 Mbps transmission data rate by using orthogonal frequency-division multiplexing (OFDM) modulation scheme. But the communication media of their system is a 2 inch metal wall which is completely different from a long pipe. Sam et al. investigates a specific concrete channel model for stress wave communications in [10]. The impulse response for a 60 inch concrete channel is tested by experiments. The maximum data rate that can be achieved by this specific channel is also evaluated based on experiment results. Unfortunately, no general channel model can be found in literature.

WUWNET'19, October 23–25, 2019, Atlanta, GA, USA

ACM ISBN 978-1-4503-7740-9/19/10…$15.00
https://doi.org/10.1145/3366486.3366508

There are several key challenges need to be tackled for SWC, which include: (a) the path loss model of stress wave propagating through a pipeline; (b) the available bandwidth that can be used for SWC; (c) stress wave channel capacity of a specific type of pipeline.

In this paper, we carefully study the propagation behavior of stress wave along a pipeline. The governing equations of stress wave propagation inside the hollow pipe are derived. The open source package GUIGUW [11] is utilized to perform mode analysis. Based on theoretical analysis and simulation results, the stress wave group velocity dispersion curves are given. We also build up a SWC system based on the commercial off-the-shelf ultrasonic piezoelectric transducer (PZT). Our salient contributions are summarized as follows.

- We detailed analyzed the propagation of stress wave along a pipeline. The mode analysis allowed us to find a specific frequency range which is most conducive to stress wave communication.
- We built up a SWC system based on a 10-feet long steel pipe and off the shelf PZTs. The communication performances were tested both in the air and underwater.
- We applied the QPSK modulation scheme to input signal. The demodulated signals showed that the stress wave channel could be established and the bit error rate (BER) was acceptable.

The rest of the paper is organized as follows. Section 2 summarizes governing equation of the stress wave propagation inside the pipeline and give the mode analysis. In Section 3, we describe our experiment platform. The software implementation of the experiment is given in Section 4. Section 5 shows the experimental results both in the air and underwater. Finally, we conclude the paper in Section 6 and provide directions for future research.

NOMENCLATURE

$\boldsymbol{b}$ or $\boldsymbol{B}$	A vector quantity is denoted by bold-faced character.
f or F	A scalar quantity is denoted by normal character.
J , I	First kind Bessel function
Y , K	Second kind Bessel function
(r, θ, z)	Cylindrical coordinate system
λ	First Lamé constants
μ	Second Lamé constants
ω	Angular frequency
ρ	Mass density
t	Time

2 PHYSICAL LAYER MODEL

In this section, we summarize the governing equation of the stress wave propagation inside the pipeline and give the mode analysis that targets a specific frequency band for stress wave communication.

2.1 Stress Wave Modeling

The stress wave propagation in an elastic or viscoelastic medium is governed by Navier's equation, which is in the form of:

$$\mu\nabla^2\mathbf{u} + (\lambda+\mu)\nabla(\nabla\cdot\mathbf{u}) = \rho\left(\frac{\partial^2\mathbf{u}}{\partial t^2}\right) \tag{1}$$

where λ and μ are the Lamé constants of the material. $\mathbf{u}$ is the displacement vector. ρ is the material density and t is time. To simplify this problem, the Helmholtz's decomposition is applied to the displacement vector in (1). The displacement vector is decomposed by a combination of scalar potential, Φ, and vector potential, $\mathbf{\Psi}$,

$$\mathbf{u} = \nabla\Phi + \nabla\times\mathbf{\Psi} \tag{2}$$

substituting (2) into (1) and using calculus identities for simple algebra, (1) can be decomposed into two equations as

$$\left(\frac{\partial^2\Phi}{\partial t^2}\right) - \left(\frac{\lambda+2\mu}{\rho}\right)\nabla^2\Phi = 0 \tag{3}$$

$$\left(\frac{\partial^2\mathbf{\Psi}}{\partial t^2}\right) - \left(\frac{\mu}{\rho}\right)\nabla^2\mathbf{\Psi} = 0 \tag{4}$$

Equation (3) and (4) fall into scalar Helmholtz equation and vector Helmholtz equation, respectively. Two additional constants c_l and c_s are defined as:

$$\begin{cases} c_l = \sqrt{\dfrac{\lambda+2\mu}{\rho}} \\ c_s = \sqrt{\dfrac{\mu}{\rho}} \end{cases} \tag{5}$$

c_l denotes the longitudinal bulk wave velocity and c_s is the shear bulk wave velocity. Let's assume that the hollow cylinder is homogeneous and infinity long. The axis of the cylinder is along the z-axis in cylindrical coordinate (r, θ, z) as shown in Fig. 1. In cylindrical system, the Laplacian terms in (3) and (4) have the following formats,

$$\begin{cases} \nabla^2\Phi = \frac{\partial^2\Phi}{\partial r^2} + \frac{1}{r}\frac{\partial\Phi}{\partial r} + \frac{1}{r^2}\frac{\partial^2\Phi}{\partial\theta^2} + \frac{\partial^2\Phi}{\partial z^2} \\ \nabla^2\mathbf{\Psi} = \left(\nabla^2\Psi_r - \frac{1}{r^2}\Psi_r - 2\frac{1}{r^2}\frac{\partial\Psi_\theta}{\partial\theta}\right)\hat{\boldsymbol{r}} \\ \quad + \left(\nabla^2\Psi_\theta - \frac{1}{r^2}\Psi_\theta - 2\frac{1}{r^2}\frac{\partial\Psi_r}{\partial\theta}\right)\hat{\boldsymbol{\theta}} + \nabla^2\Psi_z\hat{\boldsymbol{z}} \end{cases} \tag{6}$$

Combining equation (3), (4) and (6), Rose [12] presented the solutions for the potentials,

$$\begin{cases} \Phi = f(r)\, e^{-jm\theta} e^{j(\omega t - kz)} \\ \Psi_r = \psi_r(r)\, e^{-jm\theta} e^{j(\omega t - kz)}, m = 0, 1, 2\ldots \\ \Psi_\theta = \psi_\theta(r)\, e^{-jm\theta} e^{j(\omega t - kz)} \\ \Psi_z = \psi_z(r)\, e^{-jm\theta} e^{j(\omega t - kz)} \end{cases} \tag{7}$$

where the integer m is known as the circumferential order of a wave mode and k is the wavenumber. f, ψ_r, ψ_θ and ψ_z are unknown coefficients. If considering only the axisymmetric wave modes ($m = 0$), equation (7) can be simplified as,

$$\begin{cases} \Phi = f(r)\, e^{j(\omega t - kz)} \\ \mathbf{\Psi} = \boldsymbol{\psi}(r)\, e^{j(\omega t - kz)} \end{cases} \tag{8}$$

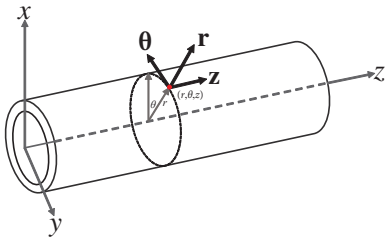

Figure 1: Hollow cylinder coordinate.

Where $\boldsymbol{\psi}(\boldsymbol{r})$ is a vector in the form of $\boldsymbol{\psi}(r) = \hat{\boldsymbol{r}}\psi_r + \hat{\boldsymbol{\theta}}\psi_\theta + \hat{\boldsymbol{z}}\psi_z$. Substituting equation (8) into (3) and (4), the solutions of partial differential equations fall into Bessel functions. In order to make the solutions as concise as possible, two intermediate variables are defined as,

$$\begin{cases} \alpha^2 = \frac{\omega^2}{c_l^2} - k^2 \\ \beta^2 = \frac{\omega^2}{c_s^2} - k^2 \end{cases} \tag{9}$$

The solutions of equation (7) are given as,

$$f(r) = \begin{cases} A_1 J_0(|\alpha| r) + B_1 Y_0(|\alpha| r) & \text{if } \omega^2/c_l^2 - k^2 \geqslant 0 \\ A_1 I_0(|\alpha| r) + B_1 K_0(|\alpha| r) & \text{if } \omega^2/c_l^2 - k^2 < 0 \end{cases} \tag{10}$$

$$\psi_r(r) = \begin{cases} A_2 J_1(|\alpha| r) + B_2 Y_1(|\alpha| r) & \text{if } \omega^2/c_s^2 - k^2 \geqslant 0 \\ A_2 I_1(|\alpha| r) + B_2 K_1(|\alpha| r) & \text{if } \omega^2/c_s^2 - k^2 < 0 \end{cases} \tag{11}$$

$$\psi_\theta(r) = \begin{cases} A_3 J_1(|\alpha| r) + B_3 Y_1(|\alpha| r) & \text{if } \omega^2/c_s^2 - k^2 \geqslant 0 \\ A_3 I_1(|\alpha| r) + B_3 K_1(|\alpha| r) & \text{if } \omega^2/c_s^2 - k^2 < 0 \end{cases} \tag{12}$$

$$\psi_z(r) = \begin{cases} A_4 J_0(|\alpha| r) + B_4 Y_0(|\alpha| r) & \text{if } \omega^2/c_s^2 - k^2 \geqslant 0 \\ A_4 I_0(|\alpha| r) + B_4 K_0(|\alpha| r) & \text{if } \omega^2/c_s^2 - k^2 < 0 \end{cases} \tag{13}$$

In the above equations, (10)- (13), A_i and B_i, $i = 1, 2, 3$ and 4, are arbitrary constants. J_ν and I_ν are first kind Bessel functions, Y_ν and are K_ν second kind Bessel functions, ν is the order of Bessel function. The final solution of the displacement vector can be derived by combining equation (10)- (13) and (7) with equation (2).

2.2 Mode Analysis

Based on the solution of governing equation, Rose [12] derived the phase and group velocities as follows,

$$\begin{cases} c_p = \omega/k \\ c_g = c_p + k\frac{\partial c_p}{\partial k} \end{cases} \tag{14}$$

In (14), c_p and c_g are phase and group velocity, respectively. They are both the function of wavenumber, k.

For a hollow cylinder, there will be multiple wave forms coexisting inside the waveguide, which are known as 'modes'. Stress waves inside a cylinder can also be generally divided into three groups. These modes are labeled as L(0, m), T(0, m) and F(n, m), where n and m are integers and L, T, and F denote longitudinal, torsional and flexural type modes, respectively. In order to select the appropriate modes, mode analysis will thus allow us to target certain frequency bands that propagate mostly inside the pipe and are most conducive to communication across long distances.

The open source package GUIGUW has been used to simulate the modes distribution along frequency band. The group velocity of different modes are calculated as shown in Fig. 2. Much attention should be paid to L(0,2) mode at a frequency between 80 kHz to 120 kHz. The group velocity of L(0,2) in this frequency range is almost a constant, which means that this mode is non-dispersive and the mode shape will remain unchanged. This is beneficial for long-range communication. Furthermore, L(0,2) is the fastest mode among those modes existing in the frequency range. Thus, post-processing algorithms can be applied to eliminate the slower modes that are undesirable.

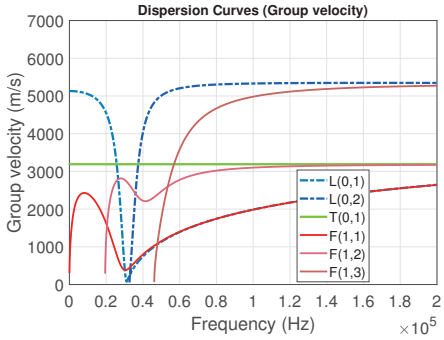

Figure 2: Group velocities of different modes along a steel pipe.

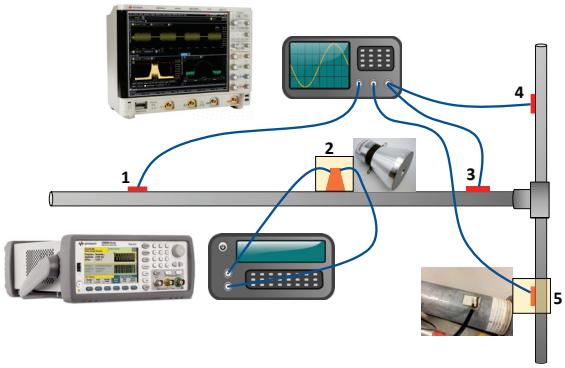

Figure 3: Schematic of the testbed.

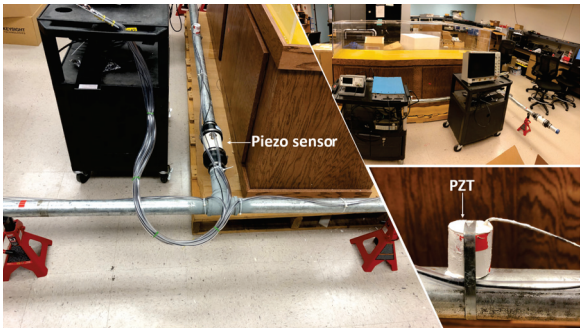

Figure 4: Real testbed in laboratory. The PZT is attached on the pipe wall using a clamp. The patch sensors are sealed inside the plastic tubes for waterproof purpose.

3 EXPERIMENT DESIGN

3.1 Stress wave tests setup

To investigate the stress wave propagation on pipeline, two galvanized steel pipes (10-ft length, 2-in diameter) are weld together and used to perform experiments. The schematic of testbed is shown in Fig. 3 and the real testbed is shown in Fig. 4. We use the piezoelectric transducer (PZT) to excite stress wave and piezoelectric discs to receive signals. In the current testbed, there is one PZT and four piezo discs.

The whole experiment process is as follows. The modulated signal is generated by signal generator (Keysight 33500B) and then sent to PZT. PZT converts the electric signal to stress wave and excites the pipeline. The vibration propagates along the pipeline and is recorded by piezo discs as long as it passes through discs. All piezo discs are connected with an oscilloscope (Keysight MSOS604), which has a high sampling rate and it is used for data acquisition. The received signals are processed by a bunch of signal processing techniques, e.g. denoising, demodulation, Fourier transform and so forth. The experiment results are compared with theoretical analysis and final conclusion can be obtained based on comparisons.

3.2 Transducer characteristics

The transducer is composed of piezoelectric elements, also known as piezoelectric stack. The transducer used as transmitter converts electrical signals into mechanical vibrations and the receiving transducer converts mechanical vibration into electrical signals. It is important to understand the transducer characteristics that determines the usable operating frequency range. The input impedance of the transducer is measured as shown in Fig. 5. In Fig. 5(a), there are multiple peaks, while Fig. 5(b) is smooth with no peak present. These peaks are known as harmonics or resonances due to its self-impedance and self-capacitance. The piezoelectric transducer is designed to excite specific frequency range, here 40 kHz, hence its frequency response looks like a filter. However, the structure of piezoelectric disc is relatively simple and it thus has a smooth frequency response.

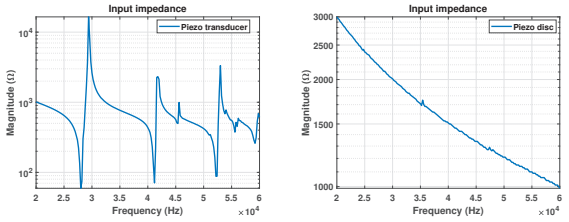

(a) Piezoelectric transducer (b) Piezoelectric discs

Figure 5: Input impedance of piezoelectric elements.

4 IMPLEMENTATION OF STRESS WAVE COMMUNICATION

Our SWC system is depiced in Fig. 4. Stress waves are generated using an off the shelf ultrasonic PZT with resonant frequency of 40 kHz. Waves are coupled into the steel pipe in the middle, and received using patch PZT sensors located on different positions as shown in Fig. 3.

The PZT actuator was driven by a QPSK pass band signal with central carrier frequency of 40 kHz, which was generated by the MATLAB/Simulink tools. The signal processing diagram was shown in Fig. 6.

The received stress wave signals were sampled and stored by an oscilloscope and then processed offline using Matlab. The communication performances are analyzed under different stress wave

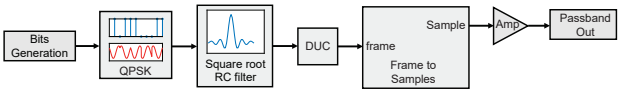

Figure 6: SWC transmitting signal generation

channel conditions with different receiver locations and surrounding environments. The processing procedure of the received signals is shown in Fig. 7.

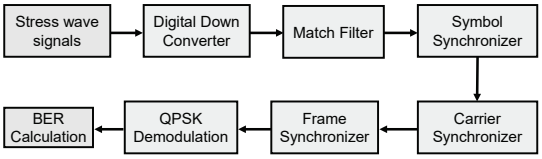

Figure 7: QPSK receiver block diagram

5 RESULTS & DISCUSSIONS

In this section, we first tested the performances of the SWC system in the lab. Afterward, the pipe setup was submerge into the seawater at a wharf in Gulveston Island. The sea test results turned out to be better than in the lab.

5.1 First Trials in the Lab

Our trail system is shown in Fig. 3. We mounted the transmitter (node 2) in the middle of the horizontal pipe. Two receivers were located on node 3 and node 4, respectively. The QPSK pass band signal with Central frequency of 40 kHz was generated to test the communication performances. The spectrual of the base band signal was shown in Fig. 8. The demodulation results on location 3 and location 4 are shown in Fig. 9.

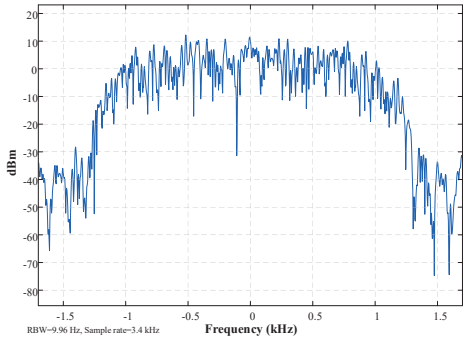

Figure 8: Spectrum analysis of QPSK signal

The BER increased dramatically after stress wave signals propagating through a join between node 3 and node 4. This is mainly due to the reflection. Specifically, when stress wave signals propagating from one pipe to another pipe, due to the impedance mismatch in the join, most of the stress wave signals will be reflected back. For

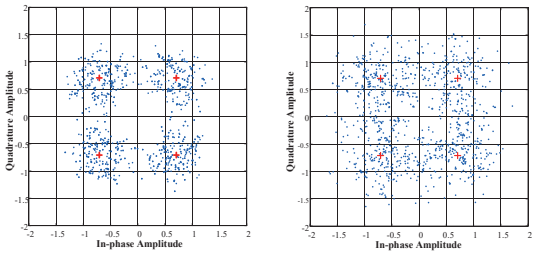

(a) Demodulation results on node 3, BER=0.0783 @ symbol rate = 1380 (b) Demodulation results on node 4, BER=0.2366 @ symbol rate = 1380

Figure 9: Demodulation results in the lab

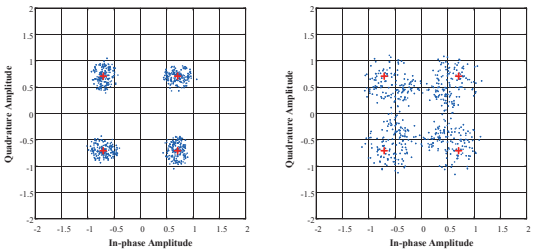

(a) Demodulation results on node 3, BER=0 @ symbol rate = 1380 (b) Demodulation results on node 4, BER=0.1127 @ symbol rate = 1380

Figure 11: Demodulation results subsea

this reason, the SNR on node 4 would be much lower than node 3 resulting in a worse BER performance.

5.2 First Trials Subsea

Our subsea test was carried out at a wharf in Gulveston Island. The pipe setup was directly submerged into the sea water as shown in Fig. 10. Then we repeated the same testing precedure as what we did in the lab. The testing results are shown in Fig. 11. It turned out that the subsea performances were much better than the lab testing results. One of the key reasons behind this was that in subsea environments the noise floor was much lower than in the air, so that the SNR of the receiving stress wave signal would be much higher subsea resulting in a much better communication performances such as much lower BER.

Figure 10: Subsea testing setup

6 CONCLUSION & FUTURE WORK

To date, peoples are still struggling on the underwater communications, since no physical signals can be utilized as the perfect information carrier in subsea environments. For example, electromagnetic signals experience fast attenuation and acoustic signals suffer from long propagation delay, limited bandwidth, and multipath problems. In this paper, we propose a new stress wave communication technology that can be deployed along the offshore pipelines which are the most popular man-made infrastructures subsea. We build up a SWC system based on two steel pipes. Both the lab and sea tests have demonstrated that a successful communication link can be established along a pipe.

Although our test bed has successfully demonstrated the stress wave communication, it can be optimized even further. First, the current carrier frequency (40kHz) was determined by the commercial off the shelf PZT, which is not within the optimal operation frequency range of a steel pipe. Second, the coupling between PZT and pipe can be further enhanced since we directly connected them together in our current system. Third, no preamplifier was applied on the receiver site. So in the future, after tackling the afford mention situations, we will fully explore the potential of SWC along a pipeline, such as the transmission range, available bandwidth, and power consumption, etc.

REFERENCES

[1] Mark J Kaiser. Offshore pipeline construction cost in the us gulf of mexico. *Marine Policy*, 82:147–166, 2017.

[2] Mark J Kaiser. Us gulf of mexico deepwater pipeline construction–a review of lessons learned. *Marine Policy*, 86:214–233, 2017.

[3] Burhan Gulbahar and Ozgur B Akan. A communication theoretical modeling and analysis of underwater magneto-inductive wireless channels. *IEEE Transactions on Wireless Communications*, 11(9):3326–3334, 2012.

[4] Hongzhi Guo, Zhi Sun, and Pu Wang. Channel modeling of mi underwater communication using tri-directional coil antenna. In *2015 IEEE Global Communications Conference (GLOBECOM)*, pages 1–6. IEEE, 2015.

[5] Debing Wei, Li Yan, Xuanheng Li, Yi Sun, Dongfeng Yuan, Jiefu Chen, and Miao Pan. Exploiting magnetic field analysis to characterize mi wireless communications in subsea environments. In *2018 International Conference on Computing, Networking and Communications (ICNC)*, pages 805–809. IEEE, 2018.

[6] Debing Wei, Li Yan, Xuanheng Li, Jie Wang, Jiefu Chen, Miao Pan, and Yahong Rosa Zheng. Ferrite assisted geometry-conformal magnetic induction antenna and subsea communications for auvs. In *2018 IEEE Global Communications Conference (GLOBECOM)*, pages 1–6. IEEE, 2018.

[7] Debing Wei, Steban S Soto, Javier Garcia, Aaron T Becker, Li Wang, and Miao Pan. Rov assisted magnetic induction communication field tests in underwater environments. In *Proceedings of the Thirteenth ACM International Conference on Underwater Networks & Systems*, page 20. ACM, 2018.

[8] Craig C Johnson. A seismic communications investigation employing a piezoelectric transducer. Technical report, SOUTHWEST RESEARCH INST SAN ANTONIO TX, 1972.

[9] Tristan J Lawry, Gary J Saulnier, Jonathan D Ashdown, Kyle R Wilt, Henry A Scarton, Sam Pascarelle, and John D Pinezich. Penetration-free system for transmission of data and power through solid metal barriers. In *2011-MILCOM 2011 Military Communications Conference*, pages 389–395. IEEE, 2011.

[10] Sam Siu, Qing Ji, Wenhao Wu, Gangbing Song, and Zhi Ding. Stress wave communication in concrete: I. characterization of a smart aggregate based concrete channel. *Smart Materials and Structures*, 23(12):125030, 2014.

[11] Paolo Bocchini, Alessandro Marzani, and Erasmo Viola. Graphical user interface for guided acoustic waves. *Journal of Computing in Civil Engineering*, 25(3):202–210, 2010.

[12] Joseph L Rose. *Ultrasonic guided waves in solid media*. Cambridge university press, 2014.